Computational Study on the Interaction of N1 Substituted Pyrazole Derivatives with B-Raf Kinase: An Unusual Water Wire Hydrogen-Bond Network and Novel Interactions at the Entrance of the Active Site

Jans H. Alzate-Morales, Ariela Vergara-Jaque, and Julio Caballero*

Centro de Bioinformática y Simulación Molecular, Universidad de Talca, 2 Norte 685, Casilla 721, Talca, Chile

Received February 3, 2010

Docking and molecular dynamics (MD) simulations of N1 substituted pyrazole derivatives complexed with B-Raf kinase were performed to gain insight into the structural and energetic preferences of these inhibitors. First, a comparative study of fully automated docking programs AutoDock, ICM, GLIDE, and Surflex-Dock in closely approximating the X-ray crystal structure of the inhibitor (1*E*)-5-[1-(4-piperidinyl)-3-(4-pyridinyl)-1*H*-pyrazol-4-yl]-2,3-dihydro-1*H*-inden-1-one oxime was performed. Afterward, the dynamics of the above-mentioned compound and the less active analogous compounds with 1-methyl-4-piperidinyl and tetrahydro-2*H*-pyran-4-yl groups at position N1 of pyrazole ring inside the B-Raf active site were analyzed by MD simulations. We found that the most active compound has stable interactions with residues Ile463 and His539 at the entrance of the B-Raf active site. Those interactions were in very good agreement with more reliable quantum mechanics/molecular mechanics calculations performed on the torsional angle φ between the pyrazole ring and the substituents at position N1. In addition, we identified a water wire connecting N2 of the pyrazole ring, Cys532, and Ser536, which is composed of three water molecules for the most active compound. We found some differences in the water wire hydrogen-bond network formed by less active compounds. We suggest that the differences between these structural features are responsible for the differences in activity among the studied compounds.

INTRODUCTION

The Ras−Raf−MEK−ERK signaling pathway is a highly conserved signaling pathway in eukaryotes critical for cell survival, growth, proliferation, and tumorigenesis. Raf kinases exist as three isoforms: A-, B-, and C-Raf; among them, B-Raf have been identified as the primary MEK activator.[1] B-Raf is one of the most frequently mutated genes in human cancers.[2] Many of the B-Raf mutations activate the kinase activity of B-Raf. Hence, therapeutic inhibition of oncogenic B-Raf kinase activity is considered a promising strategy to treat cancer.[3] In the last years, several inhibitors of B-Raf have been discovered.[4] Some of them are currently undergoing clinical evaluation, such as PLX4032,[5] XL281,[6] and GSK2118436.[7]

Computational applications have been essential for rational design of kinase inhibitors. Models that are capable to explain the interactions and predict the biological activity of compounds by their structural properties have been considered powerful tools to design highly active molecules. Computational methods, such as docking,[8,9] quantitative structure−activity relationship,[10−15] pharmacophore,[16,17] de novo design,[18,19] quantum mechanics/molecular mechanics (QM/MM),[8,15,20−22] and molecular dynamics (MD)[23] have been used for studying kinase inhibitors. These methods have been scarcely applied for studying B-Raf kinase inhibitors. One example was reported by Luo et al.[24] They carried out a high-throughput virtual screening by using docking; they identified a series of purine-2,6-dione analogues as inhibitors against B-Raf from a database that contains about 90 000 compounds. In another paper, Fratev et al.[25] used MD, free energy molecular mechanics-Poisson−Boltzmann surface area (MM-PBSA), and local-binding energy (LBE) approaches to examine the molecular basis of the inactive wild-type B-Raf and the V600E mutant inhibitions and selectivities of a series of inhibitors. As the structural basis of the B-Raf activation is still not well understood, MD simulations were used by Fratev et al.[26] and Moretti et al.[27] to explain the effect of different inactivating mutations on the conformational stability of the protein.

In a recent report, Hansen et al. synthesized substituted pyrazoles, evaluated their IC_{50} against B-Raf kinase, and tested them for cellular inhibition of the target pathway (IC_{50} of ERK phosphorylation in melanoma cells, pERK).[28] They found that compound **1** (Figure 1) is a potent B-Raf inhibitor with $IC_{50} = 0.03$ nM and pERK = 9 nM. However, small changes at the position N1 of the pyrazole ring, like in compounds **2** and **3**, lead to lesser active compounds (Figure 1). In the current work, we studied the structure−activity relationships of the above-mentioned B-Raf inhibitors by using different computational approaches. We analyzed the dynamics and energetics of the interactions of N1-substituents in the pyrazole ring with residues at the entrance of the B-Raf pocket.

* Corresponding author. Telephone: 56-71-201-685. Fax: 56-71-201-662. E-mail: jcaballero@utalca.cl or jmcr77@yahoo.com.

10.1021/ci100049h
Published on Web 06/04/2010

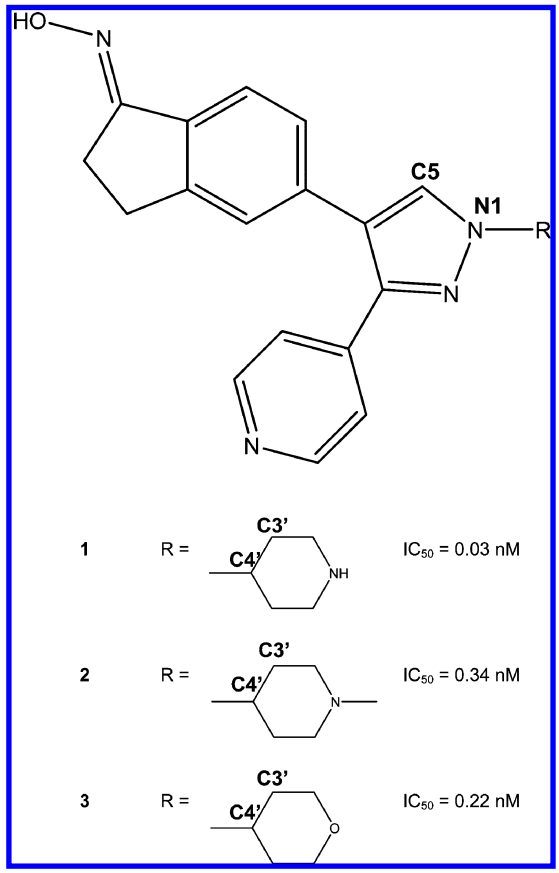

Figure 1. Pyrazole-based inhibitors and the effect of modification of the subtituent at position 1 of the pyrazole scaffold. Atoms involved in the scanned torsional angle φ are labeled.

METHODOLOGY AND COMPUTATIONAL DETAILS

Docking. In molecular docking, we attempt to predict the structure (or structures) of the intermolecular complex formed between two or more molecules. Docking has been widely used to suggest the binding modes of protein inhibitors.[29−33] Most docking algorithms are able to generate a large number of possible structures, and so they also require a means to score each structure to identify those of most interest. In general, the "docking problem" is thus concerned with the generation and evaluation of plausible structures of intermolecular complexes.

The first step in our docking study was the application of docking methodologies Autodock,[34] Glide,[35] ICM,[36] and Surflex-Dock[37] for reproducing the crystal structure of human B-Raf in a complex with compound **1** (accession code in PDB: 3d4q).

The B-Raf structure was used as a template for the docking simulations. The protein coordinates were extracted from the crystal structure of human B-Raf in the above-mentioned complex. Before the docking simulations, the protonation states of compounds were determined with the software Epik.[38] The analysis was performed at biological conditions, i.e., using water as a solvent and pH = 7.0. All obtained tautomers were further used in docking experiments. Optimized three-dimensional (3D) structures and Mulliken charges for the studied compounds were obtained by using the semiempirical quantum-chemical method AM1[39] contained in the Gaussian software package.[40] The preparation of the B-Raf protein structure included the modeling of the region encompassing residues 601−612 (12 residues), which were not solved into the crystal structures, and it was modeled using the loop building routine of Modeler.[41] The energy of the resulting loop region was refined using first 1000 steps of conjugate gradients minimization, in order to remove bad contacts, and then, a short 1000 ps long MD simulation was performed, keeping the rest of the protein residues frozen, in order to avoid disturbance of the B-Raf active site. The partial charges on protein residues were assigned according to the force field available in each docking method used.

The docking methods were compared according to root-mean-square deviation (rmsd) values. The method with lesser rmsd values was selected for carrying out further docking simulations for compounds **2** and **3**.

Autodock. AutoDock 3.0[34] uses the empirical free-energy function to evaluate binding free energies and the Lamarckian genetic algorithm (GA) to search for favorable binding positions. The grid maps defining the search region and representing the protein in the docking process were calculated with AutoGrid and had dimensions of 60 Å × 60 Å × 60 Å, with a spacing of 0.375 Å between the grid points. Each optimized ligand was located in the protein's active site for each docking run. Torsional degrees of freedom were defined with the help of AutoTors. An AutoDock protocol was applied, with an initial population of 100 randomly placed individuals, a maximum number of 1×10^6 energy evaluations, a maximum number of 3×10^4 generations, a mutation rate of 0.02, a crossover rate of 0.80, and an elitism value of 2. Twenty independent docking runs were carried out for each ligand using these parameters. The 10 best docking poses for each ligand were analyzed by examining their relative total energy scores. The best docked position was determined by comparing docking poses and considering the total energy value. Among several similar docking poses, the more energetically favorable conformation was selected.

Glide. Glide docking uses a series of hierarchical filters to find the best possible ligand binding locations in a previously built receptor grid space. The filters include a systematic search approach, which samples the positional, conformational, and orientational space of the ligand before evaluating the energy interactions of the ligand with the protein.[35] The Glide program is contained in Maestro 9.0 software.[42] We used the standard-precision (SP) module of Glide. The docking hierarchy begins with the systematic conformational expansion of the ligand, followed by placement in the receptor site. Then, minimization of the ligand in the field of the receptor is carried out using the OPLS-AA[43] force field with a distance-dependent dielectric = 2.0. After that, the lowest energy poses are subjected to a Monte Carlo (MC) procedure that samples nearby torsional minima. The best pose for a given ligand is determined by the Emodel score, while different compounds are ranked using GlideScore, a modified version of the ChemScore function of Eldridge et al.,[44] that includes terms for buried polar groups and steric clashes.

ICM. The ICM methodology[36] employs internal coordinates to optimize flexible ligands in a grid-based receptor field. Energy calculations are based on the Empirical Conformational Energy Program for Peptides 3 (ECEPP/3) force-field parameters[45] and the molecular mechanics force field (MMFF) partial charges.[46] The receptor field is represented by five potential energy maps: electrostatic,

hydrogen bond, hydrophobic, and two van der Waals terms. Global optimization is used to undertake an unbiased, all-atom, flexible docking of the ligand within the rigid binding pocket. This procedure starts with a random conformational change of the free bonds, angles, and torsions according to the biased probability Monte Carlo (BPMC) algorithm[47] followed by local energy minimization of the analytical differentiable terms. Then, the complete energy, including nondifferentiable terms, is calculated. The total energy is accepted or rejected on the basis of the Metropolis criterion,[48] and favorable conformations are allocated to a conformational stack (history mechanism) that both expels from unwanted minima and promotes the discovery of new minima. After that, the procedure starts again. The conformational sampling, based on the BPMC approach,[47] selects randomly a conformation in internal coordinate space and then makes a step to a new, random position, independent of the previous one, but according to a predefined continuous-probability distribution. It is noteworthy that, after each random step, full local minimization greatly improves the efficiency of the procedure. When energy terms have no derivatives or are very expensive to compute, a double-energy MC minimization scheme minimizes the energy with respect to the differentiable terms and calculates the full energy also using the nondifferentiable terms. This double-energy scheme allows for the incorporation of complex energy terms, such as surface-based solvation energy, into the global optimization process.

Surflex-Dock. Surflex 2.1.1 is contained in the Sybyl 7.3.[49] Surflex generates putative poses for molecular fragments using a surface-based molecular similarity method.[37] This method employs the empirical Hammerhead scoring function[50] and uses an idealized active site ligand, or protomol, to generate ligand poses by incremental construction and a crossover procedure that combines pieces from distinct poses. The protomol represents a set of molecular fragments that characterizes the active site and to which the ligand of interest is fragmented and checked for both similarity and alignment.[51] Two relevant factors that significantly affect the size and extent of the protomol generated are "proto_thresh", which determines how far the protomol extends into the concavity of the target site, and "proto_bloat", which impacts how far the protomol extends outside of the concavity. In our experiments, "proto_thresh" was set to 0.2 and "proto_bloat" was left at 0 for all generated protomols, and all other parameters were left at the default values.

MD Simulations. Molecular dynamics of compounds **1**−**3** inside the B-Raf active site were studied using the OPLS-AA force field in explicit solvent with the SPC water model (OPLS-AA/SPC),[52] within the Desmond[53,54] package for MD simulations. The initial coordinates for the MD calculations were taken from the docking experiments. The SPC water molecules were then added (the dimensions of each orthorhombic water box were 63 Å × 69 Å × 79 Å approximately, which ensured the whole surfaces of the complexes to be covered), and the systems were neutralized by adding Cl^- counterions to balance the net charges of the systems. After the construction of the solvent environment, each complex system was composed by about 34 000 atoms. Before equilibration and long production MD simulations, the systems were minimized and pre-equilibrated using the default relaxation routine implemented in Desmond. For this, the program ran six steps composed of minimizations and short (12 and 24 ps) molecular dynamics simulations to relax the model system before performing the final long simulations. After that, a first 2 ns long equilibration MD simulation was performed on each complex system, and it was followed for a 5 ns long production MD simulation. The OPLS-2005[52] force field was used, along with the module MacroModel[55] to provide and check the necessary force field parameters for the ligands. When MacroModel performs an energy calculation, the program checks the quality of each parameter in use. Use of low-quality parameters, especially torsional ones, may result in inaccurate conformational energy differences and geometries. All, bond, angle, torsional, and impropers, checked parameters were listed as high- and medium-quality force field parameters for all ligands studied. During MD simulations, the equations of motion were integrated with a 2 fs time step in the NVT ensemble. The SHAKE algorithm was applied to all hydrogen atoms; the van der Waals cutoff was set to 9 Å. The temperature was maintained at 300 K, employing the Nosé−Hoover thermostat method with a relaxation time of 1 ps. Long-range electrostatic forces were taken into account by means of the particle-mesh Ewald (PME) approach. Data were collected every 1 ps during the MD runs. Visualization of protein−ligand complexes and MD trajectory analysis were carried out with the VMD software package.[56]

Torsional Angle Scanning by Using QM/MM Method. The last frame from long production MD simulations on each protein−ligand complex was selected to perform this study. Water solvent box and chlorine atoms were deleted from the systems in order to save computational time. The torsional angle of interest for this study is shown in Figure 1, and it defines the rotation of the substituent at the N1 position in the ligand pyrazole ring. QM/MM torsional angle scanning was performed using the module Q-Site[57] from the Schrödinger Suite of computational programs. Ligands were defined as part of the quantum mechanical region, and they were modeled at the density functional theory (DFT) level using the B3LYP/6-31G** method and basis set, respectively. The protein was defined as part of the molecular mechanics region, and it was modeled with the OPLS-2005 force field.[52] Protein residues 25 Å far from the ligand were frozen in all QM/MM calculations. Several previous works showed that residues far from this distance should not contribute importantly to the ligand's binding energy within the protein's binding site in computational condensed phase calculations.[58,59] Minimization of the MM region was performed using the conjugate gradient algorithm and an energy and gradient convergence criterion of 0.1 kcal/mol and 0.01 kcal/(mol Å), respectively. The selected coordinate was scanned from 180° to −180° with an increment value of 10° for each step. Minimization of the QM and MM regions was performed at each step in order to obtain the torsional angle energy profile for protein−ligand complexes.

RESULTS AND DISCUSSION

Docking. The ability of docking programs to reproduce the pose of compound **1,** close to that found in an X-ray complex reported in ref 28, was evaluated. As it can be observed in Figure 2, the docked structures fit in an optimal way with the inhibitor X-ray crystal structure for the four

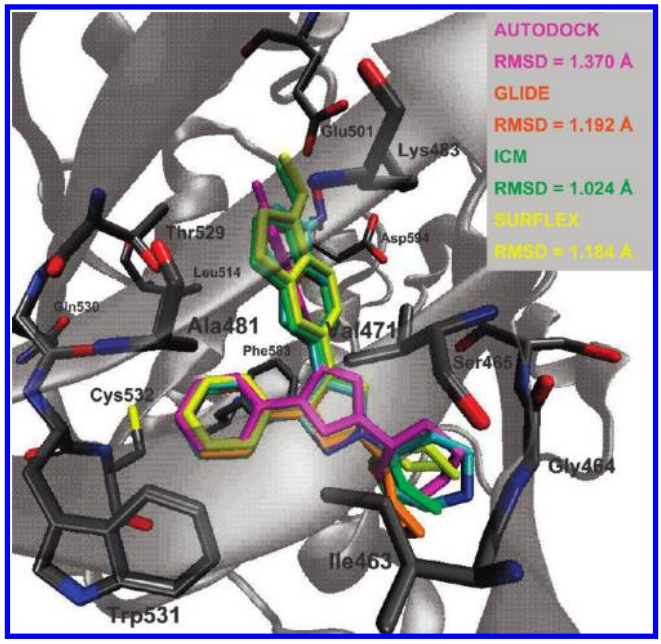

Figure 2. B-Raf/compound **1** complexes: crystallographic structure (cyan), and proposed docked structures by Autodock (magenta), Glide (orange), ICM (green), and Surflex (yellow). Hydrogens are omitted for clarity.

studied methods. The rmsd values for the docked structures with respect to the X-ray crystal inhibitor structure (all heavy atoms) were 1.370, 1.192, 1.024, and 1.184 Å using Autodock, Glide, ICM, and Surflex methods, respectively. This means that the four used docking methods could reproduce with good accuracy the position and orientation taken by compound **1** in the reported X-ray structure available in the Protein Data Bank (PDB). The best rmsd value was obtained using the ICM method, so we carried out the remaining docking experiments using this method.

Compounds **2** and **3** were docked following ICM docking protocol. Comparison of the docking results shows that, in principle, compounds **2** and **3** adopt the same binding mode identified by Hansen et al.[28] for compound **1** (Figure 3). The similar binding mode is not surprising, since all compounds contain the same scaffold and similar substituents. In all compounds:

(a) The (1*E*)-1-(hydroxyimino)-2,3-dihydro-1*H*-inden-5-yl group forms a hydrogen-bond (HB) interaction between the hydroxyimine group and Glu501, while the 2,3-dihydro-1*H*-inden-5-yl group is surrounded by Val471, Lys483, Thr529, Leu514, and Asp594.

(b) The 4-pyridinyl group is surrounded by Phe583, Ala481, Leu514, and Trp531 and forms HB interactions with the backbone of Cys532.

(c) The group at position N1 of pyrazole scaffold (R substituent in Figure 1) is at the entrance of the pocket near residues Ile463, Gly464, and Ser465.

Docking results were compared with respect to X-ray structure according to rmsd values considering groups of common atoms (Table 1). The rmsd values considering all common heavy atoms were 1.140, 1.203, and 1.118 Å for compounds **1**−**3**, respectively, which indicates that all compounds were similarly oriented. Small rmsd values (around 0.2 and 1.0 Å) were obtained considering only the pyrazole ring, the 4-pyridinyl group, or the (1*E*)-1-(hydroxyimino)-2,3-dihydro-1*H*-inden-5-yl group for all compounds,

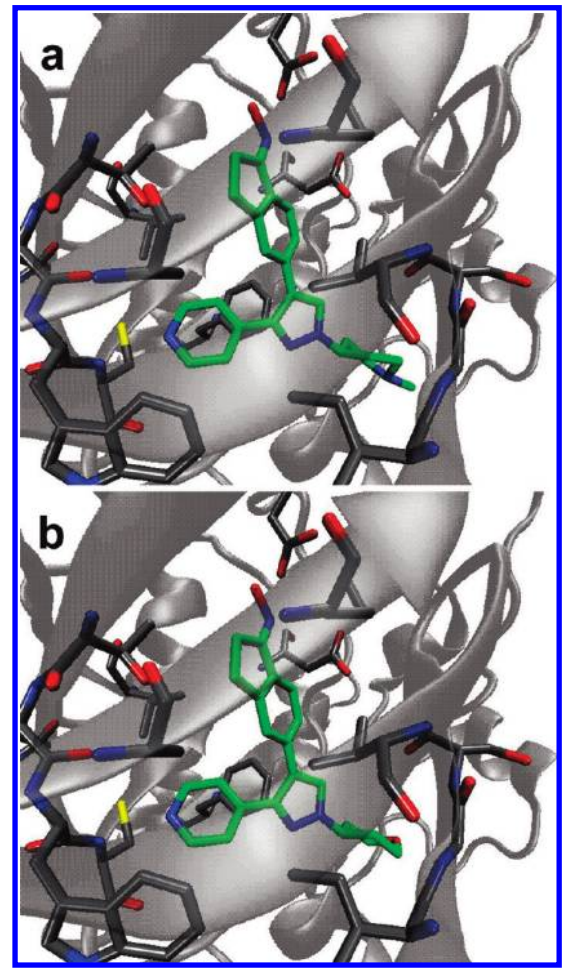

Figure 3. (a) B-Raf/compound **2** and (b) B-Raf/compound **3** complexes proposed by docking using ICM. Hydrogens are omitted for clarity.

which indicates that these parts of the molecules docked in orientations closely resembling that adopted by the crystallized molecule. The structural differences showed on the substituent at position N1 of the pyrazole ring for compounds **2** and **3** do not influence the interactions established by the groups in the rest of the molecule. However, rmsd values above 2 Å were obtained considering only common atoms in the substituent at position N1 of the pyrazole ring for compounds **1**−**3**, which indicates that groups at this position have more mobility. This sounds reasonable, considering that these groups are at the entrance of the pocket and that they are exposed in part to the water media. However, the interactions with the B-Raf residues involving these groups seem to be responsible for the differences between the inhibitory activities for compounds **1**−**3**.

MD Calculations. The most active compound **1** contains a 4-piperidinyl group at position N1 of the pyrazole scaffold, which can establish HB interactions as a HB donor. Compound **2** contains a 1-methyl-4-piperidinyl group, while compound **3** contains a tetrahydro-2*H*-pyran-4-yl group, instead of a 4-piperidinyl group, as in compound **1**. Despite the small differences in the substituents, compounds **2** and **3** have considerable differences in their activities against B-Raf with respect to compound **1** (Figure 1). The dynamics of the HB interactions between the group at position N1 of the pyrazole ring and the residues at the entrance of the B-Raf active site were studied for compounds **1**−**3** using MD

Table 1. Rmsd Values from Docking Experiments Considering Common Heavy Atoms[a]

	rmsd (Å)				
compound	all common heavy atoms	considering only pyrazole ring	considering only common atoms in substituent at position 1 of the pyrazole ring	considering only 4-pyridinyl group	considering only (1*E*)-1-(hydroxyimino)-2, 3-dihydro-1*H*-inden-5-yl group
1	1.140	0.304	2.277	0.201	0.878
2	1.203	0.506	2.287	0.258	1.012
3	1.118	0.426	2.139	0.225	0.938

[a] With respect to the X-ray structure reported in ref 28.

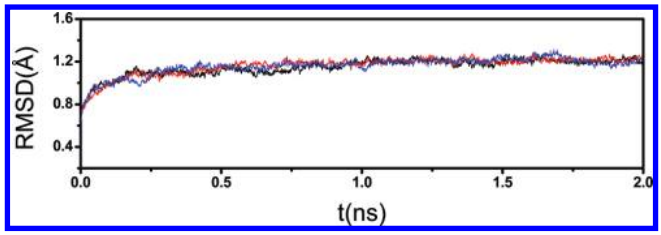

Figure 4. Time dependence of the rmsd for backbone from starting structures during equilibration process. Rmsd for systems containing compounds **1**−**3** are represented in black, red, and blue, respectively.

Table 2. Relevant Stable Distances between Atoms from the Inhibitors and B-Raf during MD Simulations

compound	D1 (Å)[a]	D2 (Å)[b]
1	2.957 ± 0.129	3.367 ± 0.150
2	2.966 ± 0.131	3.392 ± 0.150
3	2.968 ± 0.131	3.360 ± 0.147

[a] Distance between the nitrogen from both the 4-pyridinyl group and the backbone of Cys532. [b] Distance between the oxygen from the hydroxyimino group and the carboxylic carbon from the side-chain group of Glu501.

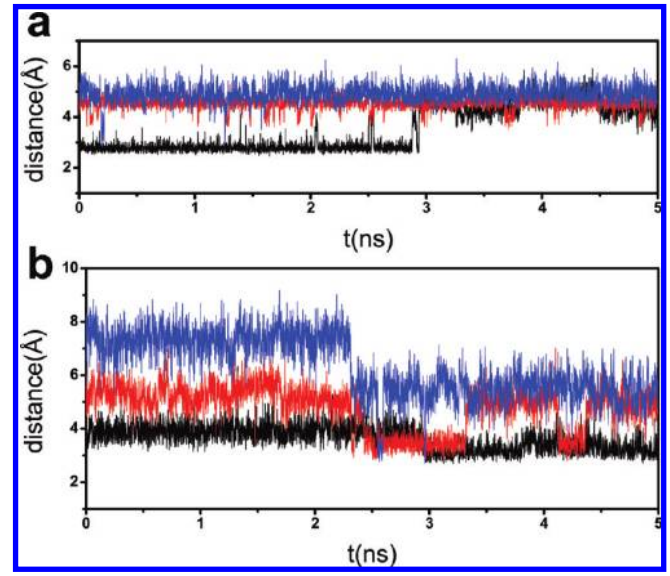

Figure 5. Distances between groups of inhibitor and residues of B-Raf for the complexes extracted from 5 ns MD simulations. (A) Distances between the atom at position 4 of the aliphatic six-member ring at position 2 of the pyrazole ring (nitrogen for compounds **1** and **2** and oxygen for compound **3**) and the backbone carbonyl group of residue Ile463 (D3). (B) Distances between the atom at position 4 of the aliphatic six-member ring at position 2 of pyrazole ring and the Nε side-chain atom of His539 (D4). Trajectories for compounds **1**−**3** are represented in black, red, and blue, respectively.

simulations. The aim is to explain the differences in the activities for these compounds.

The rmsd's of the positions for all backbone atoms from their initial configuration as a function of simulation time (the first 2 ns of equilibration MD are represented) for all of the investigated systems are shown in Figure 4. The dependences of the rmsd values were tested to check whether convergence of the calculations was obtained and whether the equilibrated MD trajectory was stable. The rmsd values remain within 1.2 Å for all systems; this demonstrates the conformational stabilities of the protein structures. Along the simulations, the studied compounds were in the expected orientations.

In all simulations, the 4-pyridinyl group at position C3 of the pyrazole ring established an HB interaction with the backbone structure of residue Cys532 and the hydroxyimino group established an HB interaction with residue Glu501. Table 2 shows that these interactions were stable during all simulations. Distance between the nitrogen from both the 4-pyridinyl group and the backbone of Cys532 (D1 in Table 2) was around 2.96 ± 0.13 Å; while the distance between the oxygen from the hydroxyimino group and the carboxylic carbon from side-chain group of Glu501 (D2 in Table 2) was around 3.36 ± 0.15 Å for all of the studied complexes. These specific interactions between B-Raf inhibitors and residues Cys532 and Glu501 have been reported before by Tsai et al.[60] in the development of inhibitor PLX4720 and by Wang et al.[61] in the development of a series of pyrazolo[1,5-α]pyrimidine analogues. According to Wang et al., the interactions with the side chain of Glu501 and the backbone NH of residue Asp594 should make an important contribution to the ligands affinity by B-Raf. Other important reported interactions within the B-Raf active site include $\pi-\pi$ stacking interactions with residues Phe583 and Trp531 established by the compound SB-590885, which is structurally similar to compounds studied here.[62] These interactions were also established by compounds **1**−**3** during their MD simulations.

We also analyzed the HBs formed between the groups at the position N1 of the pyrazole ring of the inhibitors and some residues at the entrance of B-Raf binding site. To trace the motion and the dynamics for these interactions and to determine whether the HBs were formed or broken, the interatomic distances describing them were monitored during the three developed MD simulations. Figure 5A shows the distance between the atom at position 4 of the aliphatic six-member ring at position N1 of pyrazole ring (nitrogen for compounds **1** and **2** and oxygen for compound **3**) and the backbone carbonyl group of residue Ile463 (D3) for all of the complexes. D3 takes values around 2.8 ± 0.2 Å for

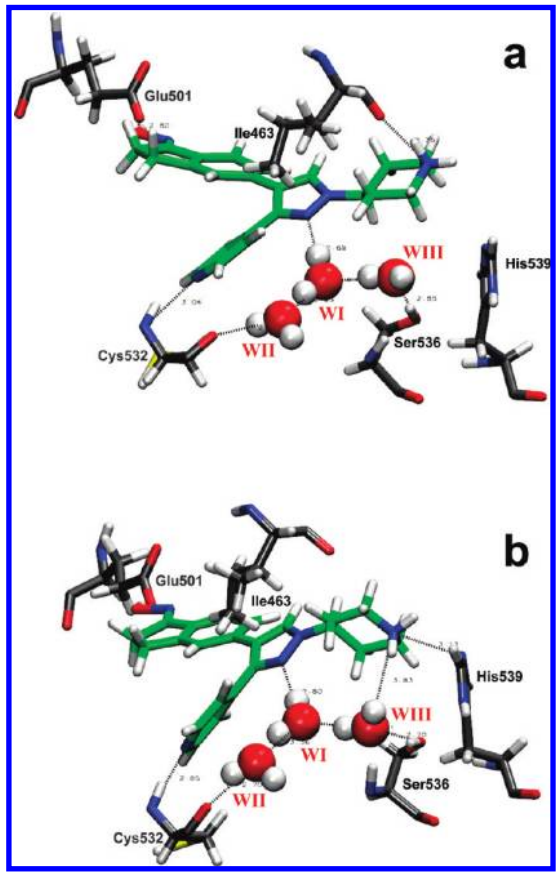

Figure 6. Hydrogen-bonding networks at the active site of the B-Raf-inhibitor complex from snapshots of the conformations obtained in 5 ns MD simulation for compound **1**: (A) from 0 to 2.9 ns and (B) from 2.9 to 5 ns.

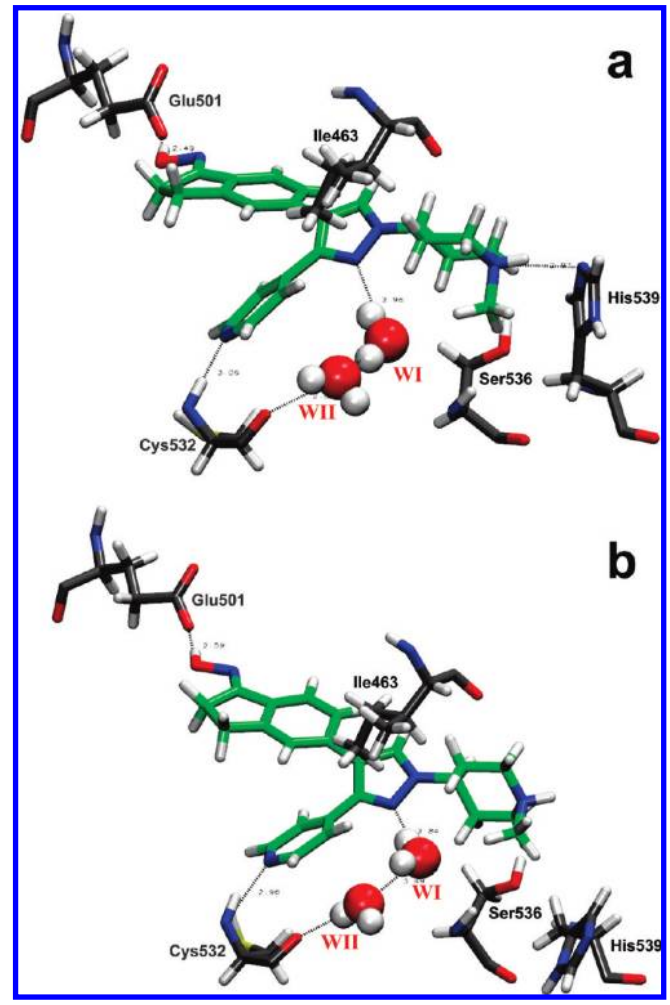

Figure 7. Hydrogen-bonding networks at the active site of the B-Raf-inhibitor complex from snapshots of the conformations obtained in 5 ns MD simulation for compound **2**: (A) when HB interactions with His539 are established and (B) when HB interactions with His539 are not established.

compound **1** until 2.9 ns, after which the interaction was broken. By contrast, it takes values above 5 Å for compounds **2** and **3** throughout their simulations. The role of residue Ile463, in the interaction with other compounds, differs somehow from the described one here, since it has been described as van der Waal's contacts with chlorine atoms.[60,61] Figure 5B shows the distance between the atom at position 4 of the aliphatic six-member ring at position N1 of the pyrazole ring and the Nε side-chain atom of His539 (D4) for all of the complexes. D4 takes values between 3 and 4.5 Å for compound **1** in most of its simulation; it takes values around 3.9 $\pm$ 0.3 Å until 2.9 ns, and after that, it takes values around 3.2 $\pm$ 0.3 Å. By contrast, D4 takes values above 4.5 Å for compounds **2** and **3** in most of their simulations. D4 takes values around 3.4 $\pm$ 0.3 Å for compound **2** between 2.5 and 3.3 ns and 4.1 and 4.3 ns, while D4 for compound **3** rarely takes values below 4 Å. According to these results, compound **1** is able to establish stable interactions with residues Ile463 (Figure 6A) and His539 (Figure 6B). Compound **2** does not interact with Ile463 and has occasional interactions with His539 (Figure 7), which suggests that the presence of methyl groups in the amine of the piperidine group obstructs the possibility of forming HBs with residues at the entrance of the pocket of B-Raf. Nitrogen of the piperidinyl ring in compound **2** occasionally interacted with the Nε side-chain atom of His539. Meanwhile, the methyl group tended to be near Cβ and Cγ of His539. This interaction was established due to a methyl group that was at the axial position on the piperidinyl ring, favoring the hydrophobic interactions and avoiding the exposition to the solvent. Finally, compound **3** does not interact with residues Ile463 and His539.

Compound **3** has a tetrahydropyran in place of the piperidine group. Protonated piperidine is a HB donor group; in this sense, it can interact with HB acceptor groups of B-Raf, such as the backbone carbonyl group of residue Ile463 and the Nε side-chain atom of His539. On the other hand, tetrahydropyran is a HB acceptor group; it should interact with HB donor groups of B-Raf. Figure 8 shows the distance between the oxygen atom from the tetrahydropyran and two HB donor groups of B-Raf for the complex with compound **3**. The distance D5 between the oxygen atom from the tetrahydropyran and the nitrogen from the NH_2 side-chain group of Asn580 occasionally had values around 3 Å until 2.3 ns; after this time, it took values above 4.5 Å. On the other hand, the distance D6 between oxygen atom from the tetrahydropyran and the oxygen from the OH side-chain group of Ser536 had values around 5.1 $\pm$ 0.3 Å until 2.3 ns; after this time, it took values around 4.1 $\pm$ 0.3 Å. According to these results, compound **3** is able to form HB interactions with the NH_2 side-chain group of Asn580 (Figure 9A), but they are not too stable. In addition, the oxygen atom from the tetrahydropyran can be located near to Ser536,

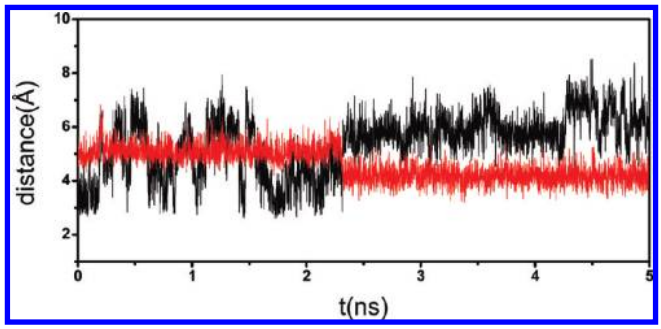

Figure 8. Distances between groups of inhibitor and residues of B-Raf for the complex B-Raf-compound **3** extracted from its 5-ns MD simulation. Distance between the oxygen from the tetrahydropyran and the nitrogen from the NH_2 side-chain group of Asn580 (D5) is represented in black. Distance between the oxygen from the tetrahydropyran and the oxygen from the OH side-chain group of Ser536 (D6) is represented in red.

without forming an HB interaction. Overall, the above-mentioned interactions with residues Ile463, His539, Asn580, and Ser536, at the entrance of the B-Raf active site, are described here for the first time. Some of them seem to be important for the achievement of high potency in compound **1** and should be used in the design of more potent and selective B-Raf inhibitors.

On the other hand, the N2 atom of pyrazole ring does not have any interactions with surrounding residues in the complex between B-Raf and compound **1**, according to Hansen et al.[28] However, the authors found that an inhibitor with a methyl group at this position lead to a marked decrease in the inhibitory activity. When compound **1** is located inside the B-Raf active site, the N2 is exposed to the water media, far from residues in the pocket. We further explored the water environment around N2. With this idea in mind, we calculated the radial distribution function (RDF) between N2 and water molecules for all complexes. Figure 10A shows these RDFs derived from MD simulations. The plots show sharp peaks centered at 2.85 Å. The presence of these peaks indicates that there is a great probability that water molecules interact with N2 forming HBs during MD simulations. A second peak appears at 4.5 or 5 Å, which suggests that other water molecules are connected to the first one. Visual inspection of the dynamics of water molecules located from 0 to 10 Å away from N2 reveals that there is a water wire connecting N2 of the pyrazole ring, Cys532, and Ser536. Figure 10B shows RDFs between the oxygen from the backbone of Cys532 and the water molecules for all complexes derived from MD simulations. These plots show peaks at 2.75 and 4.85 Å for all compounds, similar to previous peaks observed in Figure 10A. The peak at 2.75 Å indicates that there is a great probability that water molecules interact with oxygen from the backbone of Cys532 forming HBs during MD simulations. The peak at 4.85 Å is caused by water molecules which interact with N2. Figure 10C shows RDFs between the oxygen from the OH side-chain group of Ser536 and the water molecules for all complexes derived from MD simulations. Plots for complexes containing compounds **1** and **3** show peaks at 2.75 Å, which indicate that water molecules interact with OH side-chain group of Ser536 forming HBs during MD simulations for these compounds. The small peak at 2.75 Å for complex containing compound **2** indicates that there are not water molecules

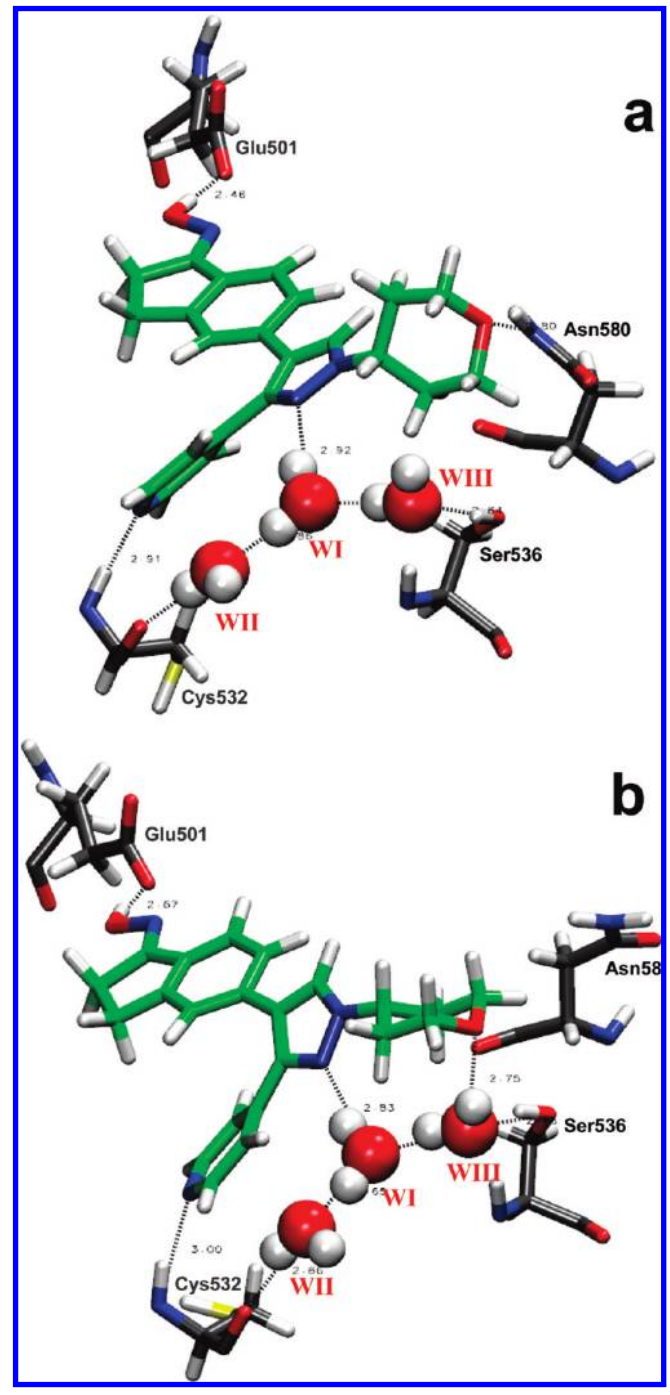

Figure 9. Hydrogen-bonding networks at the active site of the B-Raf-inhibitor complex from snapshots of the conformations obtained in 5 ns MD simulation for compound **3**: (A) when HB interactions with Asn580 are established and (B) from 2.3 to 5 ns.

forming stable HBs with Ser536 during its simulation, when this compound is inside the active site of B-Raf.

The water wires connecting N2 of the pyrazole ring, Cys532, and Ser536 for compounds **1**−**3** are shown in Figures 6, 7, and 9, respectively. We denoted the sites of the water molecules as WI, WII, and WIII as indicated in the figures. The water wire for compound **2** only contains sites WI and WII (Figure 7), since the methyl group from 1-methyl-4-piperidinyl blocks the site WIII. Figure 11A, B, and C shows the distances between the oxygen of water molecules (at sites WI−WIII) and the N2 of the pyrazole ring, the backbone of Cys532, and the OH side-chain group

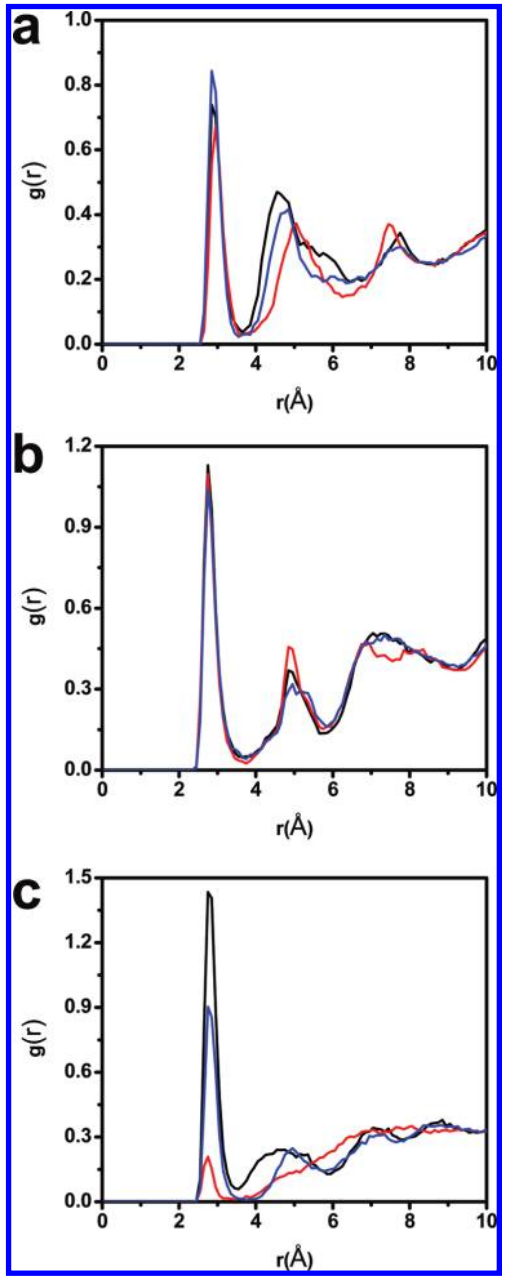

Figure 10. Water radial distribution functions: (A) from N2 of pyrazole, (B) from oxygen from the backbone of Cys532, and (C) from the oxygen from the OH side-chain group of Ser536. Distributions for compounds **1**−**3** are represented in black, red, and blue, respectively.

of Ser536, respectively, for compound **1** during its MD simulation. In these plots, when distances take values around 2.8 Å, an HB is established. The analysis of these plots reveals that several water molecules participate in each HB. When a water molecule leaves the wire, another one fills the vacant space. The water wire lasts the whole 5 ns simulation. There is only one refill of water molecules at site WI in the first part of the simulation, when compound **1** has interactions with Ile463. After that (after 2.9 ns), water molecules were rechanged four times, and the ones at site WII were rechanged three times; however, water molecules at site WIII are maintained until the end of the simulation. When the compound **1** interacts with His539 (after 2.9 ns), the water molecule at site WIII can form an additional HB with the nitrogen atom from the piperidine (Figure 6B). This

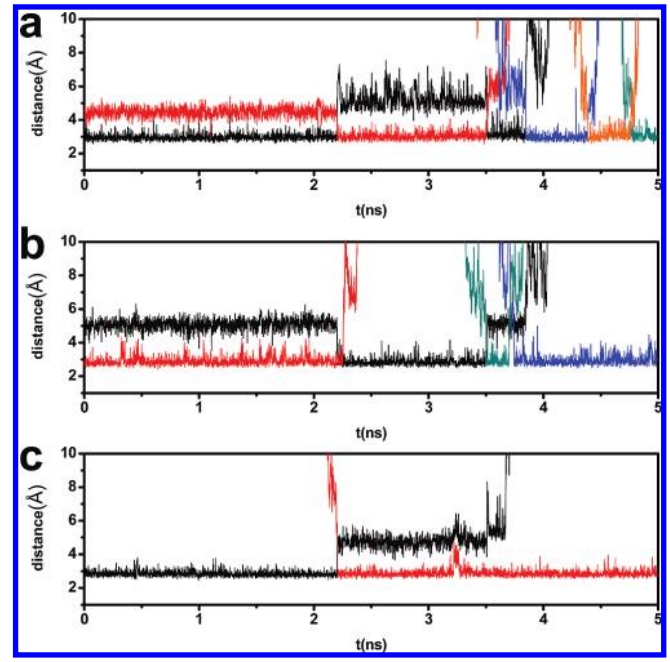

Figure 11. Distances of water molecules involved in the water wire connecting N2 of the pyrazole ring, Cys532, and Ser536 for compound **1** extracted from its 5 ns MD simulation. (A) Distances between the oxygen of water molecules and the N2 of pyrazole ring. (B) Distances between the oxygen of water molecules and the oxygen from the backbone of Cys532. (C) Distance between the oxygen of water molecules and the oxygen from the OH side-chain group of Ser536. Different colors in each plot represent different water molecules.

additional interaction might be related with the poor refill of water molecules at site WIII.

The plots of the distances between the oxygen of water molecules and the N2 of pyrazole ring, the backbone of Cys532, and the OH side-chain group of Ser536 respectively, for compounds **2** and **3,** during their MD simulation, are provided in the Supporting Information (Figures S1 and S2). Water molecules from the water wire of complex B-Raf−compound **2** were continuously changed during the 5 ns MD simulation. The water wire for complex B-Raf−compound **2** has only the sites WI and WII, while the site WIII is blocked by 1-methyl-4-piperidinyl; therefore, the HB network is smaller for this complex, and the methyl group obstructs the interaction of compound **2** with residue Ser536. Additionally, the presence of a hydrophobic group might harm the stability of the water wire. Water molecules from the water wire of complex B-Raf−compound **3** were continuously changed at site WI until 2.3 ns, when the inhibitor has occasionally interactions with Asn580; in this period of time, the interactions at site WII and WIII are stable. After 2.3 ns, when compound **3** is close to Ser536, the oxygen atom from tetrahydropyran is able to interact with the OH side-chain group of Ser536 mediated by the water molecule at site WIII (Figure 9B). The water molecules from sites WI and WIII were renewed only once during this period; however, water molecules at site WII were continuously changed. As it happened for compound **1**, an additional HB with the oxygen atom from the tetrahydropyran (Figure 9B) might be related with the poor refill of water molecules at site WIII. Figure 12 shows the distances between water molecules at site WIII and the oxygen from the tetrahydropyran for the complex B-Raf−compound **3** extracted from

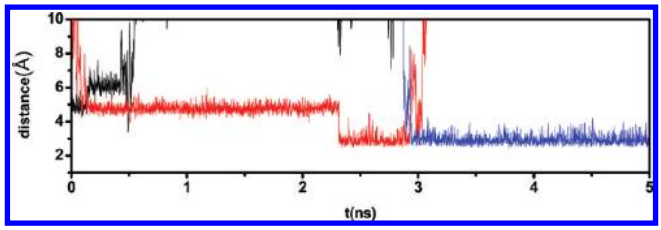

Figure 12. Distances between the water molecules at site WIII and the oxygen from the tetrahydropyran for the complex B-Raf−compound **3** extracted from its 5 ns MD simulation.

its 5 ns MD simulation. The studied distances take values around 4.8 ± 0.2 Å until 2.3 ns, when the oxygen atom from the tetrahydropyran has occasionally interactions with Asn580; after that it takes values around 2.9 ± 0.2 Å, which means that an HB between the tetrahydropyran from the inhibitor and the water molecule at site WIII is established. The analysis of the water mediated interactions, by means of RDF and MD, between the N2 atom of the pyrazole ring and the residues Cys532 and Ser536 suggests the significance of the described water wire in the stability and potency showed by B-Raf inhibitory compounds studied, and it confirms the well-known importance of the solvent in protein−ligand interactions. A HB donor or acceptor group attached at position N2 of the pyrazole ring should target the interaction with residues Cys532 and Ser536, respectively, and should have impact in the improvement in potency and selectivity of new B-Raf inhibitors.

Water molecules with a peculiar dynamics were identified at sites WI−WIII, forming a water wire. Such water molecules exchange with external solvent, but other water molecules occupy the mentioned positions during all the MD simulations. Sites WI−WIII are located at the entrance of the active site, this facilitates the exchange. According to our results, these water molecules are not structural waters, since they occupy transient cavities at the entrance of the pocket.[63]

To evaluate the stability of the proposed interactions, the MD for the complex B-Raf−compound **1** was extended to 10 ns. When the simulation was extended for additional 5 ns, the HB interaction of the 4-pyridinyl group at position C3 of the pyrazole ring, with the backbone structure of residue Cys532, and the HB interaction of the hydroxyimino group and the residue Glu501 were completely stable. The distances D3 and D4 extracted from the range between 5 and 10 ns are shown in the Supporting Information (Figure S3). D3 returned to take values around 2.8 Å at certain intervals, which indicates that compound **1** is able to recover its interaction with Ile463. On the other hand, D4 continued to have values between 3 and 4.5 Å in most of its simulation. In addition, the distances between the oxygen of water molecules (at sites WI−WIII) and the N2 of pyrazole ring, the backbone of Cys532, and the OH side-chain group of Ser536, respectively, for compound **1** during the range between 5 and 10 ns of its MD simulation are shown in the Supporting Information (Figure S4). We verified that the water wire lasted the whole 10 ns simulation. As in the previous part of the simulation, water molecules were less exchanged when compound **1** interacts with Ile463, and water molecule at site WIII was the least refilled.

QM/MM Torsional Angle Scanning. The groups at position N1 of the pyrazole ring have a great mobility. According to MD results, the HB interactions that they have with residues in their surroundings, dictate the existence of some preferred conformations. These conformations also become stable due to the presence of the water molecules at site WIII of the water wire. We obtained a detailed picture of these conformations by MD simulations in water media. To complement this study, we carried out a conformational search by rotating the torsional angle φ between the pyrazole ring and the substituent at position N1 (torsional angle C5−N1−C4′−C3′ as represented in Figure 1). For this, we analyzed the energy profiles of protein−ligand QM/MM optimized structures, where the inhibitor was treated at a high level of theory with DFT using the method and the basis set B3LYP/6-31G**, and residues of the whole B-Raf protein were treated with molecular mechanics using the OPLS-2005 force field. For purposes of saving computational time, the explicit solvent water molecules were not used during this analysis.

We compared the conformations obtained by using QM/MM torsional angle scanning with the previously obtained ones by using MD. Figure 13 shows the plot of the QM/MM energies against the studied torsional angle φ and the distribution of φ from the 5 ns MD simulations for the three compounds. The torsional angle scanning for compound **1** shows a minimum at $\varphi = 20°$. This minimum includes conformations with the charged amine group of the piperidine from the inhibitor having a HB interaction with the backbone carbonyl group of residue Ile463. Furthermore, the plot also shows minima at −170° and 140°. These minima include conformations with the charged amine group having interactions with His539. On the other hand, distribution of φ from the 5 ns MD simulation shows a sharp peak at $\varphi = 30°$ and several broad peaks at $\varphi = -150$, −60, and 150°. These peaks include conformations having interactions with Ile463 and His539, respectively. Since torsional angle scanning was carried out without considering the solvent, some differences should be expected; however, conformations having interactions with residues Ile463 and His539 were obtained by both methods.

The QM/MM torsional angle scanning for compound **2** shows minima between $\varphi = 30$ and 110°. These minima include conformations with the amine group of the 1-methyl-4-piperidinyl from the inhibitor having an HB interaction with His539. Furthermore, the plot also shows a minimum at −170°. This minimum includes conformations where the 1-methyl-4-piperidinyl group does not interact with any residue. Distribution of φ from the 5 ns MD simulation for the same compound shows only one broad peak at $\varphi = 140°$. This peak includes conformations having interactions with His539, and the ones which do not interact with any residue at the entrance of the pocket. The scanning for compound **3** shows a minimum at $\varphi = -110°$. This minimum includes conformations with the oxygen atom from the tetrahydropyran from the inhibitor having an HB interaction with the nitrogen from the NH_2 side-chain group of Asn580. Furthermore, it also shows a minimum at −120°. This minimum includes conformations where the oxygen from the tetrahydropyran does not have interactions with B-Raf residue but is located near the residue Ser536. Distribution of φ from the 5 ns MD simulation for the same compound shows two peaks: one at $\varphi = -70°$ and the other at $\varphi = 150°$. In the first peak, conformations which interact with residue Asn580

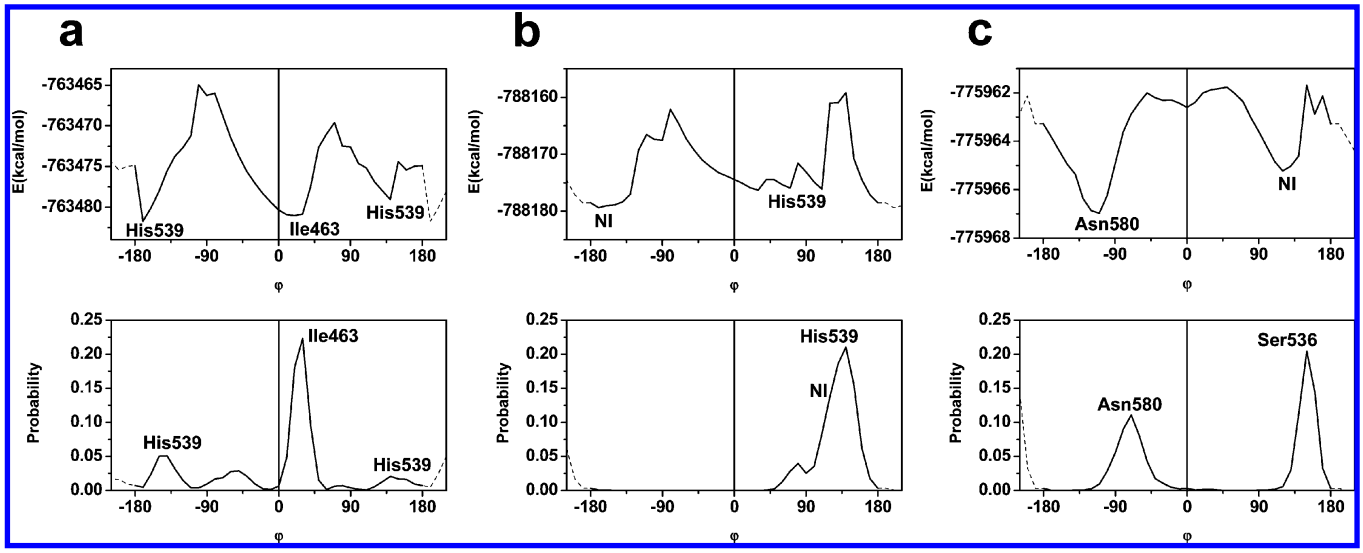

Figure 13. Torsional angle scanning by using QM/MM (up) and distribution from 5 ns MD simulations (bottom) of torsional angle C5−N1−C4′−C3′ (φ) in the binding site of B-Raf: (A) for compound **1**, (B) for compound **2**, and (C) for compound **3**. Minima from the scanning and peaks from the distribution are labeled with the residue in contact with the inhibitor. NI means that there are not interactions with any residue.

and conformations which do not have interaction with any residue are included, whereas the second peak include conformations which have interaction with Ser536 mediated by a water molecule.

The QM/MM scanning experiments were able to predict the conformations of minimal energy adopted by the rotation of the groups at position N1 of the pyrazole ring from the inhibitors. They were in good agreement with and confirmed the results obtained by MD simulations.

CONCLUSIONS

Molecular docking methods were used to predict the orientation of three pyrazole derivatives within the B-Raf binding site. All the docking methods (Autodock, Glide, ICM, and Surflex) reproduced the previously reported position of compound **1** within B-Raf's active site. The remaining compounds were oriented in a similar manner. The groups at position N1 of the pyrazole ring showed the major difference with respect to the reported crystal structure (estimated by rmsd values considering only common atoms in substituent at position N1 of the pyrazole ring for each inhibitor). The differences between these groups are responsible of the differences in the inhibitory activities of the studied compounds. For this reason, we studied the dynamics of the complexes.

MD simulations were carried out to study the dynamics of the inhibitors and the interactions with residues in the B-Raf active site. We found some aspects that can help to understand why the piperidinyl group has better interactions at the entrance of the pocket than other similar groups.

The most active inhibitor (compound **1**) shows interactions at the entrance of the B-Raf active site between the piperidinyl group of the inhibitor and the residues Ile463 and His539. In addition, the N2 of the pyrazole ring has interactions with Cys532 and Ser536 mediated by water molecules forming a water wire, which is dynamically stable. The water wire is formed by three sites: WI, WII, and WIII, which are always occupied by water molecules during the MD simulation. The charged amine group from piperidine can form an hydrogen-bond (HB) interaction with the water molecule at site WIII.

Compound **2** shows relatively stable interactions at the entrance of the B-Raf active site between the 1-methyl-4-piperidinyl group of the inhibitor and the residue His539. In the complex, the N2 of the pyrazole ring has interactions with Cys532 mediated by water molecules forming a water wire, which is dynamically stable. The water wire for the complex of compound **2** does not include the residue Ser536 because the methyl group blocks the site WIII.

Compound **3** establishes occasionally interactions at the entrance of the B-Raf active site between the tetrahydropyran group of the inhibitor and the residue Asn580. As in compound **1**, the N2 of the pyrazole ring of compound **3** has interactions with Cys532 and Ser536 mediated by water molecules forming a water wire, which is also dynamically stable. The water wire has the three above-mentioned sites, which are always occupied by water molecules during the MD simulation. The oxygen from tetrahydropyran can establish an HB interaction with the water molecule at site WIII.

The inhibitor−B-Raf interactions described above were corroborated by using a more accurate quantum mechanics/molecular mechanics (QM/MM) torsional angle scanning method, where the inhibitor was treated with density functional theory (DFT) methodology and the protein was modeled using OPLS-2005 force field.

The computational approaches used in this study, allowed us to understand the importance of some residues at the entrance of the B-Raf active site in the achievement of potency for compounds studied. The residues His539, Ile463, and Ser536, located at the entrance of the active site, should be good target candidates in the future development of more potent and selective B-Raf inhibitors.

ACKNOWLEDGMENT

J.H.A.M. acknowledges the financial support through a postdoctoral fellowship PDS-086 from PBCT and the

Government of Chile. J.C. thanks "Becas Universidad de Talca" for financial support through a doctoral fellowship.

Supporting Information Available: Distances of water molecules involved in the water wire connecting N2 of pyrazole ring, Cys532, and Ser536 for compounds **2** (Figure S1) and **3** (Figure S2) extracted from their 5 ns MD simulations. Distances between groups of inhibitor and residues of B-Raf for the complex B-Raf−compound **1** (Figure S3), and distances of water molecules involved in the water wire (Figure S4) extracted from the range between 5 and 10 ns of its MD simulation. This information is available free of charge via the Internet at http://pubs.acs.org.

REFERENCES AND NOTES

(1) Mercer, K. E.; Pritchard, C. A. Raf proteins and cancer: B-Raf is identified as a mutational target. *Biochim. Biophys. Acta* **2003**, *1653*, 25–40.

(2) Garnett, M. J.; Marais, R. Guilty as charged: B-RAF is a human oncogene. *Cancer Cell* **2004**, *6*, 313–319.

(3) Li, N.; Batt, D.; Warmuth, M. B-Raf kinase inhibitors for cancer treatment. *Curr. Opin. Invest. Drugs* **2007**, *8*, 452–456.

(4) Ramnath, N.; Adjei, A. Inhibitors of Raf kinase and MEK signaling. *Update Cancer Ther.* **2007**, *2*, 111–118.

(5) Safety Study of PLX4032 in Patients With Solid Tumors. *Clinical Trials*; National Institutes of Health: Bethesda, MD; ClinicalTrials.gov; Identifier: NCT00405587.

(6) Study of XL281 in Adults With Solid Tumors. *Clinical Trials*; National Institutes of Health: Bethesda, MD; ClinicalTrials.gov; Identifier: NCT00451880.

(7) A Phase I Study to Investigate the Safety, Pharmacokinetics, and Pharmacodynamics of GSK2118436 in Subjects With Solid Tumors. *Clinical Trials*; National Institutes of Health: Bethesda, MD; ClinicalTrials.gov; Identifier: NCT00880321.

(8) Alzate-Morales, J. H.; Caballero, J.; Vergara-Jaque, A.; González-Nilo, F. D. Insights into the structural basis of N2 and O6 substituted guanine derivatives as cyclin-dependent kinase 2 (CDK2) inhibitors: prediction of the binding modes and potency of the inhibitors by docking and ONIOM calculations. *J. Chem. Inf. Model.* **2009**, *49*, 886–899.

(9) Larsen, C. A.; Bisson, W. H.; Dashwood, R. H. Tea Catechins Inhibit Hepatocyte Growth Factor Receptor (MET Kinase) Activity in Human Colon Cancer Cells: Kinetic and Molecular Docking Studies. *J. Med. Chem.* **2009**, *52*, 6543–6545.

(10) Fernandez, M.; Tundidor-Camba, A.; Caballero, J. Modeling of Cyclin-Dependent Kinase Inhibition by 1H-Pyrazolo[3,4-d]Pyrimidine Derivatives Using Artificial Neural Network Ensembles. *J. Chem. Inf. Model.* **2005**, *45*, 1884–1895.

(11) González, M.; Caballero, J.; Helguera, A.; Garriga, M.; González, G.; Fernández, M. 2D Autocorrelation Modelling of the Inhibitory Activity of Cytokinin-Derived Cyclin-Dependent Kinase Inhibitors. *Bull. Math. Biol.* **2006**, *68*, 735–751.

(12) Caballero, J.; Fernández, M.; Saavedra, M.; González-Nilo, F. D. 2D Autocorrelation, CoMFA, and CoMSIA modeling of protein tyrosine kinases' inhibition by substituted pyrido[2,3-d]pyrimidine derivatives. *Bioorg. Med. Chem.* **2008**, *16*, 810–821.

(13) Caballero, J.; Fernández, M.; González-Nilo, F. D. Structural requirements of pyrido[2,3-d]pyrimidin-7-one as CDK4/D inhibitors: 2D autocorrelation, CoMFA and CoMSIA analyses. *Bioorg. Med. Chem.* **2008**, *16*, 6103–6115.

(14) Gueto, C.; Ruiz, J. L.; Torres, J. E.; Méndez, J.; Vivas-Reyes, R. Three-dimensional quantitative structure-activity relationship studies on novel series of benzotriazine based compounds acting as Src inhibitors using CoMFA and CoMSIA. *Bioorg. Med. Chem.* **2008**, *16*, 2439–2447.

(15) Alzate-Morales, J.; Caballero, J. Computational Study of the Interactions between Guanine Derivatives and Cyclin-Dependent Kinase 2 (CDK2) by CoMFA and QM/MM. *J. Chem. Inf. Model* **2010**, *50*, 110–122.

(16) Muthas, D.; Sabnis, Y. A.; Lundborg, M.; Karlén, A. Is it possible to increase hit rates in structure-based virtual screening by pharmacophore filtering? An investigation of the advantages and pitfalls of post-filtering. *J. Mol. Graph. Model.* **2008**, *26*, 1237–1251.

(17) Xie, H. Z.; Li, L. L.; Ren, J. X.; Zou, J.; Yang, L.; Wei, Y.; Yang, S. Y. Pharmacophore modeling study based on known spleen tyrosine kinase inhibitors together with virtual screening for identifying novel inhibitors. *Bioorg. Med. Chem. Lett.* **2009**, *19*, 1944–1949.

(18) Uno, M.; Ban, H. S.; Nabeyama, W.; Nakamura, H. de novo Design and synthesis of N-benzylanilines as new candidates for VEGFR tyrosine kinase inhibitors. *Org. Biomol. Chem.* **2008**, *6*, 979–981.

(19) Vieth, M.; Erickson, J.; Wang, J.; Webster, Y.; Mader, M.; Higgs, R.; Watson, I. Kinase Inhibitor Data Modeling and de Novo Inhibitor Design with Fragment Approaches. *J. Med. Chem.* **2009**, *52*, 6456–6466.

(20) Alzate-Morales, J. H.; Contreras, R.; Soriano, A.; Tuñon, I.; Silla, E. A Computational Study of the Protein-Ligand Interactions in CDK2 Inhibitors: Using Quantum Mechanics/Molecular Mechanics Interaction Energy as a Predictor of the Biological Activity. *Biophys. J.* **2007**, *92*, 430–439.

(21) Gleeson, M. P.; Gleeson, D. QM/MM As a Tool in Fragment Based Drug Discovery. A Cross-Docking, Rescoring Study of Kinase Inhibitors. *J. Chem. Inf. Model.* **2009**, *49*, 1437–1448.

(22) Alzate-Morales, J. H.; Caballero, J.; Gonzalez-Nilo, F. D.; Contreras, R. A computational ONIOM model for the description of the H-bond interactions between NU2058 analogues and CDK2 active site. *Chem. Phys. Lett.* **2009**, *479*, 149–155.

(23) Villacañas, O.; Pérez, J. J.; Rubio-Martínez, J. Structural Analysis of the Inhibition of Cdk4 and Cdk6 by p16INK4a Through Molecular Dynamics Simulations. *J. Biomol. Struct. Dynamics* **2002**, *20*, 347–358.

(24) Luo, C.; Xie, P.; Marmorstein, R. Identification of BRAF Inhibitors through In Silico Screening. *J. Med. Chem.* **2008**, *51*, 6121–6127.

(25) Fratev, F.; Jónsdóttir, S.; Ó.; Mihaylova, E.; Pajeva, I. Molecular Basis of Inactive B-RAFWT and B-RAFV600E Ligand Inhibition, Selectivity and Conformational Stability: An in Silico Study. *Mol. Pharmaceutics* **2009**, *6*, 144–157.

(26) Fratev, F.; Jonsdottir, S. An in silico study of the molecular basis of B-RAF activation and conformational stability. *BMC Struct. Biol.* **2009**, *9*, 47.

(27) Moretti, S.; De Falco, V.; Tamburrino, A.; Barbi, F.; Tavano, M.; Avenia, N.; Santeusanio, F.; Santoro, M.; Macchiarulo, A.; Puxeddu, E. Insights into the molecular function of the inactivating mutations of B-Raf involving the DFG motif. *Biochim. Biophys. Acta, Mol. Cell Res.* **2009**, *1793*, 1634–1645.

(28) Hansen, J. D.; Grina, J.; Newhouse, B.; Welch, M.; Topalov, G.; Littman, N.; Callejo, M.; Gloor, S.; Martinson, M.; Laird, E.; Brandhuber, B. J.; Vigers, G.; Morales, T.; Woessner, R.; Randolph, N.; Lyssikatos, J.; Olivero, A. Potent and selective pyrazole-based inhibitors of B-Raf kinase. *Bioorg. Med. Chem. Lett.* **2008**, *18*, 4692–4695.

(29) Hou, T.; Zhang, W.; Xu, X. Molecular docking studies of a group of hydroxamate inhibitors with gelatinase-A by molecular dynamics. *J. Comput.-Aided Mol. Des.* **2002**, *16*, 27–41.

(30) Zaheer-ul-haq; Wellenzohn, B.; Liedl, K. R.; Rode, B. M. Molecular Docking Studies of Natural Cholinesterase-Inhibiting Steroidal Alkaloids from Sarcococca saligna. *J. Med. Chem.* **2003**, *46*, 5087–5090.

(31) Rojo, L. E.; Alzate-Morales, J.; Saavedra, I. N.; Davies, P.; Maccioni, R. B. Selective Interaction of Lansoprazole and Astemizole with Tau Polymers: Potential New Clinical Use in Diagnosis of Alzheimer's Disease. *J. Alzheimer's Dis.* **2010**, *19*, 573–589.

(32) Pedretti, A.; Villa, L.; Vistoli, G. Modeling of Binding Modes and Inhibition Mechanism of Some Natural Ligands of Farnesyl Transferase Using Molecular Docking. *J. Med. Chem.* **2002**, *45*, 1460–1465.

(33) Caballero, J.; Vergara-Jaque, A.; Fernández, M.; Coll, D. Docking and quantitative structure-activity relationship studies for sulfonyl hydrazides as inhibitors of cytosolic human branched-chain amino acid aminotransferase. *Mol. Diversity* **2009**, *13*, 493–500.

(34) Morris, G. M.; Goodsell, D. S.; Halliday, R. S.; Huey, R.; Hart, W. E.; Belew, R. K.; Olson, A. J. Automated docking using a Lamarckian genetic algorithm and an empirical binding free energy function. *J. Comput. Chem.* **1998**, *19*, 1639–1662.

(35) Friesner, R. A.; Banks, J. L.; Murphy, R. B.; Halgren, T. A.; Klicic, J. J.; Mainz, D. T.; Repasky, M. P.; Knoll, E. H.; Shelley, M.; Perry, J. K.; Shaw, D. E.; Francis, P.; Shenkin, P. S. Glide: A New Approach for Rapid, Accurate Docking and Scoring. 1. Method and Assessment of Docking Accuracy. *J. Med. Chem.* **2004**, *47*, 1739–1749.

(36) Abagyan, R.; Totrov, M.; Kuznetsov, D. ICM - A new method for protein modeling and design: Applications to docking and structure prediction from the distorted native conformation. *J. Comput. Chem.* **1994**, *15*, 488–506.

(37) Jain, A. N. Surflex: Fully Automatic Flexible Molecular Docking Using a Molecular Similarity-Based Search Engine. *J. Med. Chem.* **2003**, *46*, 499–511.

(38) *Epik*, version 1.5; Schrödinger, LLC: New York, NY, 2007.

(39) Dewar, M. J. S.; Zoebisch, E. G.; Healy, E. F.; Stewart, J. J. P. Development and use of quantum mechanical molecular models. 76. AM1: a new general purpose quantum mechanical molecular model. *J. Am. Chem. Soc.* **1985**, *107*, 3902–3909.

(40) Frisch, M. J. Trucks, G. W.; Schlegel, H. B.; Scuseria, G. E.; Robb, M. A.; Cheeseman, J. R.; Montgomery, J. A., Jr.; Vreven, T.; Kudin, K. N.; Burant, J. C.; Millam, J. M.; Iyengar, S. S.; Tomasi, J.; Barone, V.; Mennucci, B.; Cossi, M.; Scalmani, G.; Rega, N.; Petersson, G. A.; Nakatsuji, H.; Hada, M.; Ehara, M.; Toyota, K.; Fukuda, R.; Hasegawa, J.; Ishida, M.; Nakajima, T.; Honda, Y.; Kitao, O.; Nakai, H.; Klene, M.; Li, X.; Knox, J. E.; Hratchian, H. P.; Cross, J. B.; Bakken, V.; Adamo, C.; Jaramillo, J.; Gomperts, R.; Stratmann, R. E.; Yazyev, O.; Austin, A. J.; Cammi, R.; Pomelli, C.; Ochterski, J. W.; Ayala, P. Y.; Morokuma, K.; Voth, G. A.; Salvador, P.; Dannenberg, J. J.; Zakrzewski, V. G.; Dapprich, S.; Daniels, A. D.; Strain, M. C.; Farkas, O.; Malick, D. K.; Rabuck, A. D.; Raghavachari, K.; Foresman, J. B.; Ortiz, J. V.; Cui, Q.; Baboul, A. G.; Clifford, S.; Cioslowski, J.; Stefanov, B. B.; Liu, G.; Liashenko, A.; Piskorz, P.; Komaromi, I.; Martin, R. L.; Fox, D. J.; Keith, T.; Al-Laham, M. A.; Peng, C. Y.; Nanayakkara, A.; Challacombe, M.; Gill, P. M. W.; Johnson, B.; Chen, W.; Wong, M. W.; Gonzalez, C.; Pople, J. A. *Gaussian 03*Gaussian, Inc.: Wallingford, CT, 2004.

(41) Fiser, A.; Sali, A. Modeller: Generation and Refinement of Homology-Based Protein Structure Models. *Methods Enzymol.* **2003**, *374*, 461–491.

(42) *Maestro*, version 9.0; Schrödinger, LLC: New York, NY, 2007.

(43) Jorgensen, W. L.; Maxwell, D. S.; Tirado-Rives, J. Development and Testing of the OPLS All-Atom Force Field on Conformational Energetics and Properties of Organic Liquids. *J. Am. Chem. Soc.* **1996**, *118*, 11225–11236.

(44) Eldridge, M. D.; Murray, C. W.; Auton, T. R.; Paolini, G. V.; Mee, R. P. Empirical scoring functions: I. The development of a fast empirical scoring function to estimate the binding affinity of ligands in receptor complexes. *J. Comput.-Aided Mol. Des.* **1997**, *11*, 425–445.

(45) Nemethy, G.; Gibson, K. D.; Palmer, K. A.; Yoon, C. N.; Paterlini, G.; Zagari, A.; Rumsey, S.; Scheraga, H. A. Energy parameters in polypeptides. 10. Improved geometrical parameters and nonbonded interactions for use in the ECEPP/3 algorithm, with application to proline-containing peptides. *J. Phys. Chem.* **1992**, *96*, 6472–6484.

(46) Halgren, T. A. Merck molecular force field V. Extension of MMFF94 using experimental data, additional computational data, and empirical rules. *J. Comput. Chem.* **1996**, *17*, 616–641.

(47) Abagyan, R.; Totrov, M. Biased Probability Monte Carlo Conformational Searches and Electrostatic Calculations for Peptides and Proteins. *J. Mol. Biol.* **1994**, *235*, 983–1002.

(48) Metropolis, N.; Rosenbluth, A. W.; Rosenbluth, M. N.; Teller, A. H.; Teller, E. Equation of State Calculations by Fast Computing Machines. *J. Chem. Phys.* **1953**, *21*, 1087–1092.

(49) *SYBYL*, version 7.3; Tripos Inc.: St Louis, MO.

(50) Jain, A. N. Scoring noncovalent protein-ligand interactions: A continuous differentiable function tuned to compute binding affinities. *J. Comput.-Aided Mol. Des.* **1996**, *10*, 427–440.

(51) Jain, A. Surflex-Dock 2.1: Robust performance from ligand energetic modeling, ring flexibility, and knowledge-based search. *J. Comput.-Aided Mol. Des.* **2007**, *21*, 281–306.

(52) Kaminski, G. A.; Friesner, R. A.; Tirado-Rives, J.; Jorgensen, W. L. Evaluation and Reparametrization of the OPLS-AA Force Field for Proteins via Comparison with Accurate Quantum Chemical Calculations on Peptides†. *J. Phys. Chem. B* **2001**, *105*, 6474–6487.

(53) *Desmond Molecular Dynamics System*, version 2.2;; D. E. Shaw Research, Schrödinger, LLC: New York, NY, 2009.

(54) Bowers, K. J.; Chow, E.; Xu, H.; Dror, R. O.; Eastwood, M. P.; Gregersen, B. A.; Klepeis, J. L.; Kolossvary, I.; Moraes, M. A.; Sacerdoti, F. D.; Salmon, J. K.; Shan, Y.; Shaw, D. E. In *Proceedings of the 2006 ACM/IEEE conference on Supercomputing*; ACM: Tampa, FL, 2006; p 84.

(55) *MacroModel*, version 9.5; Schrödinger, LLC: New York, NY, 2007.

(56) Humphrey, W.; Dalke, A.; Schulten, K. VMD Visual molecular dynamics. *J. Mol. Graph.* **1996**, *14*, 33–38.

(57) *QSite*, version 5.5; Schrödinger, LLC: New York, NY, 2009.

(58) Soriano, A.; Silla, E.; Tuñón, I.; Ruiz-López, M. F. Dynamic and Electrostatic Effects in Enzymatic Processes. An Analysis of the Nucleophilic Substitution Reaction in Haloalkane Dehalogenase. *J. Am. Chem. Soc.* **2005**, *127*, 1946–1957.

(59) Ruiz-Pernia, J. J.; Tuñon, I.; Moliner, V.; Hynes, J. T.; Roca, M. Dynamic Effects on Reaction Rates in a Michael Addition Catalyzed by Chalcone Isomerase. Beyond the Frozen Environment Approach. *J. Am. Chem. Soc.* **2008**, *130*, 7477–7488.

(60) Tsai, J.; Lee, J. T.; Wang, W.; Zhang, J.; Cho, H.; Mamo, S.; Bremer, R.; Gillette, S.; Kong, J.; Haass, N. K.; Sproesser, K.; Li, L.; Smalley, K. S. M.; Fong, D.; Zhu, Y.; Marimuthu, A.; Nguyen, H.; Lam, B.; Liu, J.; Cheung, I.; Rice, J.; Suzuki, Y.; Luu, C.; Settachatgul, C.; Shellooe, R.; Cantwell, J.; Kim, S.; Schlessinger, J.; Zhang, K. Y. J.; West, B. L.; Powell, B.; Habets, G.; Zhang, C.; Ibrahim, P. N.; Hirth, P.; Artis, D. R.; Herlyn, M.; Bollag, G. Discovery of a selective inhibitor of oncogenic B-Raf kinase with potent antimelanoma activity. *Proc. Natl. Acad. Sci. U.S.A.* **2008**, *105*, 3041–3046.

(61) Wang, X.; Berger, D. M.; Salaski, E. J.; Torres, N.; Hu, Y.; Levin, J. I.; Powell, D.; Wojciechowicz, D.; Collins, K.; Frommer, E. Discovery of highly potent and selective type I B-Raf kinase inhibitors. *Bioorg. Med. Chem. Lett.* **2009**, *19*, 6571–6574.

(62) King, A. J.; Patrick, D. R.; Batorsky, R. S.; Ho, M. L.; Do, H. T.; Zhang, S. Y.; Kumar, R.; Rusnak, D. W.; Takle, A. K.; Wilson, D. M.; Hugger, E.; Wang, L.; Karreth, F.; Lougheed, J. C.; Lee, J.; Chau, D.; Stout, T. J.; May, E. W.; Rominger, C. M.; Schaber, M. D.; Luo, L.; Lakdawala, A. S.; Adams, J. L.; Contractor, R. G.; Smalley, K. S.; Herlyn, M.; Morrissey, M. M.; Tuveson, D. A.; Huang, P. S. Demonstration of a Genetic Therapeutic Index for Tumors Expressing Oncogenic BRAF by the Kinase Inhibitor SB-590885. *Cancer Res.* **2006**, *66*, 11100–11105.

(63) García, A. E.; Hummer, G. Water penetration and escape in proteins. *Proteins* **2000**, *38*, 261–272.

CI100049H